

An eddy covariance mesonet to measure the effect of forest age on land–atmosphere exchange

MICHAEL L. GOULDEN*†, GREGORY C. WINSTON*, ANDREW M. S. McMILLAN*, MARCY E. LITVAK*‡¹, EDWARD L. READ*, ADRIAN V. ROCHA* and J. ROBERT ELLIOT*

*Department of Earth System Science, University of California, Irvine, CA 92697, USA, †Department of Ecology and Evolutionary Biology, University of California, Irvine, CA 92697, USA, ‡School of Biological Sciences, University of Texas, Austin, TX, USA

Abstract

We deployed a mesonet of year-round eddy covariance towers in boreal forest stands that last burned in ~1850, ~1930, 1964, 1981, 1989, 1998, and 2003 to understand how CO₂ exchange and evapotranspiration change during secondary succession. We used MODIS imagery to establish that the tower sites were representative of the patterns of secondary succession in the region, and Landsat images to show that the individual stands have changed over the last 22 years in ways that match the spatially derived trends. The eddy covariance towers were well matched, with similar equipment and programs, which maximized site-to-site precision and allowed us to operate the network in an efficient manner. The six oldest sites were fully operational for ~90% of the growing season and ~70% of the dormant season from 2001 or 2002 to 2004, with most of the missing data caused by low battery charge or bad signals from the sonic anemometers. The rates of midday growing-season CO₂ uptake recovered to preburn levels within 4 years of fire. The seasonality of land–atmosphere exchange and growing-season length changed markedly with stand age. The foliage in the younger stands (1989, 1998, and 2003 burns) was almost entirely deciduous, which resulted in comparatively short growing seasons that lasted ~65 days. In contrast, the older stands (1850, 1930, 1964, and 1981) were mostly evergreen, which resulted in comparatively long growing seasons that lasted ~130 days. The eddy covariance mesonet approach we describe could be used within the context of other ecological experimental designs such as controlled manipulations and gradient comparisons.

Keywords: black spruce, boreal forest, chronosequence, fire, land–atmosphere exchange, NEE, *Picea mariana*, secondary succession, space for time

Received 19 January 2006 and accepted 9 May 2006

Introduction

Researchers have an incomplete understanding of how and why land–atmosphere exchange varies as ecosystems recover from past disturbance. Several conceptual models have been proposed that predict large changes in carbon, energy, and hydrological balance during succession (Odum, 1969; Bormann & Likens, 1979; Gorham *et al.*, 1979; Sprugel, 1985; Waring & Schlesinger, 1985; Chapin *et al.*, 2002), but data to fully test

these models have been unavailable (Thornton *et al.*, 2002; Pregitzer & Euskirchen, 2004). The significance of past disturbance is especially apparent in the boreal forest, where crown fires occur at individual locations about once every 100 years, resulting in a mosaic of large patches at different stages of succession (Fig. 1; Van Cleve *et al.*, 1986; Bonan & Shugart, 1989; Kasischke & Stocks, 2000). These patches probably differ in CO₂ and energy exchange, and observations from a single site are unlikely to be representative of an entire region. Reliable determination of regional land–atmosphere exchange requires a consideration of how exchange varies during secondary succession (Rapalee *et al.*, 1998; Kasischke & Stocks, 2000; Schulze *et al.*, 2000; Litvak *et al.*, 2003), but understanding of these patterns is still developing.

Correspondence: Michael Goulden, Department of Earth System Science, University of California, Irvine, CA 92697-3100, USA, tel. +1 949 824 1983, e-mail: mgoulden@uci.edu

¹Present address: Department of Biology, University of New Mexico, Albuquerque, NM, USA.

Secondary succession plays out over decades and centuries, which presents a challenge for determining how the exchanges of water, energy and carbon vary during recovery. Many studies of succession use a chronosequence, or space-for-time design, where a series of well-matched sites, which presumably differ only in time since disturbance, are studied. The chronosequence design is useful for studying the complete secondary succession of ecosystems with long-lived organisms, though it is not without weakness. In particular, chronosequence studies are often challenged on: (1) the representativeness of study sites and (2) the validity of the space-for-time substitution. Chronosequences provide a key tool for understanding succession, but new methods are needed to allow investigators to evaluate the representativeness of sites and the validity of the space-for-time substitution.

Eddy covariance is a useful tool for measuring the exchanges of energy and CO₂ between land surfaces and the atmosphere (Baldochi *et al.*, 1988; Wofsy *et al.*, 1993). A series of eddy covariance towers deployed along a chronosequence might markedly improve understanding of how exchange varies with stand age, but, until recently, micrometeorologists have tended to focus more on understanding how individual sites work rather than understanding how a series of sites differ. This is partly a result of the time and cost required to operate a single eddy covariance site. If the operation of just a few sites consumes an entire lab's effort, then it would be unwise for a lab to try to operate a dozen sites. Several research groups have recently initiated chronosequence studies using eddy covariance (Amiro, 2001; Law *et al.*, 2001; Roser *et al.*, 2002; Litvak *et al.*, 2003; Clark *et al.*, 2004; Kolari *et al.*, 2004; Humphreys *et al.*, 2006), though progress has been slowed by the cost and difficulty of operating a large number of towers. The ideal approach might mimic the meteorological community's mesonet approach, where matched instruments are deployed to maximize site-to-site precision, spatial distribution, and the economy of scale (Brock *et al.*, 1995). A mesonet of eddy covariance sites deployed along a chronosequence could be used to understand how land-atmosphere exchange varies with succession, but further methodological development is needed to fully realize this potential.

We designed and deployed a small mesonet of seven year-round eddy covariance towers along a fire recovery chronosequence of boreal forest stands in central Manitoba, Canada to understand how CO₂ exchange and evapotranspiration change during secondary succession. In this paper, we describe a scalable design for eddy covariance stations that exploits several economies of scale to allow the deployment and operation of an eddy covariance mesonet. Additionally, we use remote

sensing imagery to determine whether our tower sites were representative of the patterns of secondary succession in the area and also to test the space-for-time substitution. Finally, we analyze data collected by the mesonet to determine how rapidly midday net CO₂ exchange recovers following catastrophic fire and how the phenology and seasonality of land-atmosphere exchange vary with stand age. A second paper describes how and why ecosystem carbon balance changes during succession (Goulden *et al.*, in preparation).

Mesonet design considerations

Economy of scale

Past research with eddy covariance has focused on understanding individual sites, whereas our goal was to understand the differences and similarities among seven sites arrayed across a landscape. Our success depended on establishing an economy of scale for the operation of eddy covariance towers, a goal we achieved by: (1) fully matching the towers, so that identical equipment and programs were used at all sites, and (2) designing a data acquisition architecture so that data collection and calculation were automated. The economy of scale allowed us to operate and maintain seven towers year round with an average staff of 1.5 people, though a crew of as many as six was required during installation and takedown.

Chronosequence site selection

The forests in central Manitoba are well suited for eddy covariance; the region is generally level and the burns are large (Fig. 1). We selected sites that were closely matched with respect to soil, type of most recent disturbance, topography, and climate (Jenny, 1941). Provisional tower locations were selected using Landsat imagery, burn history information from Manitoba Natural Resources, aerial photographs, and topographic maps. Precise tower locations were chosen during site visits to maximize site-to-site consistency in soil drainage (moderate to well drained) and fetch from uniform areas. The ages of the older stand were estimated by coring several black spruce at a height of 0.3 m and adding 5 years to the number of rings to account for the approximate age black spruce reaches 0.3 m height.

Our seven sites were in various stages of secondary succession following large stand replacement fires that occurred in 2003, 1998, 1989, 1981, 1964, ~1930, and ~1850 (Table 1). Six of the stands were within ~30 km of each other in the BOREAS Northern Study Area, located west of Thompson, Manitoba (Sellers *et al.*, 1997). These sites were close enough to experience

Table 1 Study sites

	Location	Conditions in summer 2005
UCI-2003*	55°53'53" 98°12'58"	Rapidly developing herbaceous layer of wild rose (<i>Rosa</i> spp.), fireweed (<i>Epilobium angustifolium</i> L.), grass, Labrador tea (<i>Ledum groenlandicum</i> Oeder), alder (<i>Alnus crispa</i>), willow (<i>Salix</i> spp.), poplar, and aspen (<i>Populus tremuloides</i> Michx). Many 2–4 cm tall black spruce (<i>Picea mariana</i>) and jack pine (<i>Pinus banksiana</i> Lamb.) seedlings. Almost all of the black spruce trees killed in the 2003 fire were still standing
UCI-1998	56°38'9" 99°56'54"	Thick, patchy layer of fireweed, wild rose, grass, Labrador tea, alder, and patchy firemoss. Many 10–25 cm tall black spruce. Almost all of the black spruce trees killed in the 1998 fire were still standing
UCI-1989	55°55'0" 98°57'52"	Thick layer of wild rose, grass, Labrador tea, fireweed, alder, and willow. Extensive firemoss with patches of sphagnum (<i>Sphagnum</i> spp.) and feather (<i>Ptilium</i> , <i>Pleurozium</i> , or <i>Hylocomium</i> spp.) moss. Many 20–100 cm tall black spruce, 100–200 cm tall jack pine, and 50–400 cm tall aspen. Most black spruce trees killed by the 1989 fire fell from 2000 to 2005
UCI-1981	55°51'47" 98°29'6"	Dense stand of 500 cm tall jack pine with scattered 500 cm tall aspen. Many 100–200 cm tall black spruce. Continuous ground cover of grass, Labrador tea, willow, and wild rose. Mix of sphagnum and feather moss. Most black spruce trees killed by the 1981 fire had fallen before 2000
UCI-1964	55°54'21" 98°22'56"	Moderately dense stand of 500–700 cm tall jack pine and aspen, with significant mortality and thinning. Many 200–600 cm tall black spruce. Ground cover of feather moss with sparse grass
UCI-1930	55°54'21" 98°31'29"	Closed canopy of 12–20 m tall black spruce, with a few senescent jack pine and aspen. Nearly 100% feather moss cover. Significant shrub layer of alder, willow, and Labrador tea
UCI-1850	55°52'45" 98°29'2"	Closed canopy of 14–18 m tall black spruce. Nearly 100% feather moss cover. Open understory with a few alders, Labrador tea, and willow

*University of California, Irvine site that last burned in 2003.

similar weather. The 1850 site was ~400 m west of the BOREAS Northern Study Area Old Black Spruce tower (NOBS; Table 2). The 1998 burn was 120 km to the northwest of the other sites. The younger sites (2003, 1998, 1989, 1981, and 1964 burns) were mostly black spruce before burning, as determined by the woody debris that remained from the fires. These stands were a mix of herbs, shrubs, aspen, black spruce, and jack pine in 2005, and were expected to return to black spruce as they mature. The older stands (1930 and 1850 burns) were dominated by closed-canopy black spruce with well-developed moss layers (both sphagnum and feathermoss). Litvak *et al.* (2003) and Bond-Lamberty *et al.* (2004) provide further details on nearby stand characteristics (Table 2).

Site access

The terrain in central Manitoba is generally level, with meandering streams and rivers, large boggy areas, and a mix of old forest stands with dense vegetation and young stands with piles of coarse woody debris. There are few roads in the area, and most of the region is inaccessible except by foot, snowmobile in winter, boat along waterways in summer, and helicopter during favorable weather (Fig. 1). Our study sites were 500–5000 m from the nearest roads, and we installed ~2000 kg of equipment at each site. We accessed

the sites during normal operation by foot or snowshoe along a network of existing and new trails. We used helicopters to transport equipment into the sites during the main site installation and takedown. The combined use of helicopters to transport heavy equipment during brief periods and foot trails for access during routine site maintenance and observation allowed us to operate sites that were up to 5 km from the road while minimizing impact and cost.

Power

The sites were 50 km or more from the nearest sources of line power (Fig. 1), which forced us to rely on solar power. The study region is at 56°N, and the winter days are short with a peak solar elevation of ~10°. We dealt with the difficult winter radiation regime in several ways. We conserved energy by reducing the overall system load to approximately 50 W. We designed the solar power array with 1000 W of panels, creating a situation where less than 2 h of full sunlight a day was required to fully operate a system. We mounted the panels vertically on a secondary scaffold tower that rose above the trees. The panels had a clear view to the southern horizon, which maximized the charge during the winter and had the added benefit of shedding snow. Finally, we designed the systems to actively manage the load based on the charge state of the batteries.

Table 2 Nearby study sites on well- to moderately well-drained clay soil (see also Sellers *et al.*, 1997)

	Available data sets	Selected references	Location relative to current sites	Comparison to current sites
NOBS*	10 years of eddy covariance and ecological measurements from BOREAS, Harvard University, and the University of Wisconsin (UW)	Goulden <i>et al.</i> (1997), Dunn <i>et al.</i> (2006), Gower <i>et al.</i> (1997), Cohen <i>et al.</i> (2003)	NOBS tower is 400 m east of UCI-1850	NOBS tower samples both well- and poorly drained areas. UCI-1850 tower is centered in a well-drained deciduous and larger area
UW-D1998 [†]	Extensive ecological measurements	Bond-Lamberty <i>et al.</i> (2004)	3 km south of UCI-1998	Wetter with more sphagnum moss than UCI-1998
UW-D1989	Extensive ecological measurements	Bond-Lamberty <i>et al.</i> (2004)	1.5 km southwest of UCI-1989	Similar vegetation, steeper, and more southerly aspect than UCI-1989
UW-D1981	Extensive ecological measurements	Bond-Lamberty <i>et al.</i> (2004)	75 m east of UCI-1981	Similar to UCI-1981
UW-D1964	Extensive ecological measurements	Bond-Lamberty <i>et al.</i> (2004)	1.5 km northwest of UCI-1964	More deciduous, larger trees than UCI-1964
UW-D1930	Extensive ecological measurements	Bond-Lamberty <i>et al.</i> (2004)	500 m northeast of UCI-1930	Similar to UCI-1930
UW-D1850	Extensive ecological measurements	Bond-Lamberty <i>et al.</i> (2004)	400 m east of UCI-1850	Similar to UCI-1850
UCI-Litvak-1989 [‡]	1–2 months of tower data, biomass	Litvak <i>et al.</i> (2003)	1.5 km southwest of UCI-1989	Similar vegetation, steeper, and more southerly aspect than UCI-1989
UCI-Litvak-1981	1–2 months of tower data, biomass	Litvak <i>et al.</i> (2003)	500 m east of UCI-1981	More deciduous and less jack pine than UCI-1981
UCI-Litvak-1964	1–2 months of tower data, biomass	Litvak <i>et al.</i> (2003)	1.5-km northwest of UCI-1964	More deciduous and larger trees than UCI-1964
UCI-Litvak-1930	1–2 months of tower data, biomass	Litvak <i>et al.</i> (2003)	500 m northeast of UCI-1930	Similar to UCI-1930

*Northern Old Black Spruce site.

[†]University of Wisconsin, dry site that last burned in 1998.

[‡]University of California, Irvine site that last burned in 1989 and that was occupied by Litvak *et al.* (2003).

The operation of all the equipment was under the control of a data logger, which monitored the voltage of the battery bank and switched on and off various components when the voltage crossed prescribed thresholds.

Open vs. closed-path gas analyzer

A key decision was the selection of infrared gas analyzer (IRGA). Open-path IRGAs have become popular recently, with several durable and precise instruments on the market. An open path uses less power than the combination of a closed-path IRGA and pump. Open

paths respond rapidly to changes in gas concentration, eliminating the need to correct for the underestimation of high frequency fluctuations. However, open paths must be calibrated by hand, precluding automated calibration, and are susceptible to signal degradation from obstructions in the optical path. Most significantly, the density correction (Webb *et al.*, 1980; referred to as the WPL correction hereafter), which is needed to account for the correlations between vertical wind, CO₂ concentration, and air density, is much larger for open paths than closed paths. We decided to use closed path IRGAs based on theoretical considerations and a pilot study.

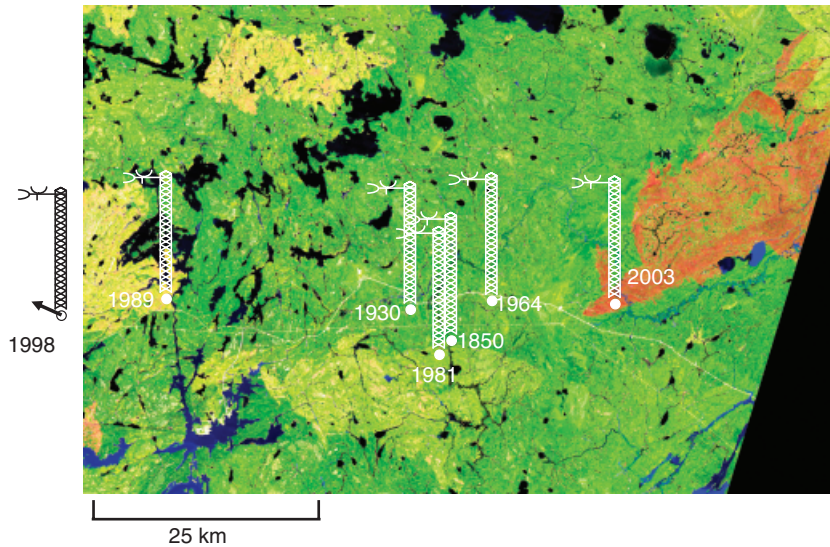


Fig. 1 Landsat 5 Thematic Mapper image for 06/07/2005 showing flux tower locations and years of most recent burn. The image is false color (bands 5, 4, 3 are RGB). Dense vegetation appears as green, water appears as blue or black, and bare soil or dead plant material appear as red. Mature black spruce forest is green; recently burned area is red; partially recovered areas are on a gradient from red to yellow to green. A dirt highway (Provincial Road 391) and power line traverse the image from east to west.

The true CO_2 flux (F_{CO_2}) is the difference between the raw measured CO_2 flux ($F_{\text{CO}_2, \text{raw}}$) and a correction term ($F_{\text{CO}_2, \text{WPL correction}}$):

$$F_{\text{CO}_2} = F_{\text{CO}_2, \text{raw}} - F_{\text{CO}_2, \text{WPL correction}} \quad (1)$$

The correction term increases with increasing latent and, especially, sensible heat flux (H). A cursory examination of Eq (1) indicates the uncertainty associated with the WPL correction will be greatest when $|F_{\text{CO}_2, \text{WPL correction}}| \gg |F_{\text{CO}_2}|$ and comparatively unimportant when $|F_{\text{CO}_2, \text{WPL correction}}| \leq |F_{\text{CO}_2}|$. In other words, F_{CO_2} will be highly uncertain during periods when it is the small difference between two much larger terms. Data collected previously at NOBS (Goulden *et al.*, 1997) indicated $|F_{\text{CO}_2, \text{WPL correction}}|$ would far exceed $|F_{\text{CO}_2}|$ during many periods. Intervals when F_{CO_2} is much less than $1 \mu\text{mol m}^{-2} \text{s}^{-1}$ and H is much greater than 100 W m^{-2} are especially common during daylight periods in the boreal spring (March and April), and result in a $|F_{\text{CO}_2, \text{WPL correction}}|$ that exceeds $|F_{\text{CO}_2}|$ by a factor of 10–100. Given the uncertainty in H and, hence, $F_{\text{CO}_2, \text{WPL correction}}$, we questioned whether reliable measurements of CO_2 flux during light periods in the boreal spring would be possible with an open-path IRGA.

The difficulty of using an open-path IRGA to make year-round flux measurements in a boreal forest was underscored by a pilot study during winter 2000–2001. The WPL-corrected F_{CO_2} determined with an open-path IRGA (LI-7500, LiCor, Lincoln, NE, USA) frequently indicated CO_2 uptake despite extreme cold (uptake of

up to $3\text{--}4 \mu\text{mol m}^{-2} \text{s}^{-1}$ at air temperatures below -20°C ; data not shown). Parallel measurements with a closed-path IRGA did not indicate uptake, underscoring the potential for open-path IRGAs to produce spurious data during the boreal dormant season. Other groups have also observed that open-path IRGAs may indicate significant carbon uptake during periods when photosynthesis is unlikely, possibly as a result of the generation of a local sensible heat flux from the sensor head (Burba *et al.*, 2005). Our overarching goal was to make reliable observations year round, and we, therefore, selected a closed-path IRGA.

Temperature control

The winter weather in Manitoba is severe, with nighttime low temperatures from -30 to -40°C . Our decision to use a closed-path IRGA necessitated that we maintain an instrument enclosure above 0°C . We achieved this goal by insulating the walls of the instrument boxes so that the temperatures inside the boxes remained 20°C above the temperatures outside the boxes when all the equipment was operating. We then buried the boxes in the soil and moss and under the snow, which buffered the temperature immediately outside the boxes at 0 to -10°C . The overall effect was to maintain the temperatures inside of the boxes at $10\text{--}20^\circ\text{C}$ throughout the winter solely using the waste energy generated by the IRGA and pump. We

removed the insulation from the boxes during summer to prevent overheating.

Data telemetry, data storage, sampling rate

The sites were remote (Fig. 1), and access, especially during winter, was difficult and sometimes dangerous. Given the expense of field operation, we opted to maintain the sites from our home university in California, approximately 3000 km to the southwest. Despite this distance, we kept a close eye on the equipment by relaying a subset of the field data in near real time to our lab using the GOES satellite. These data were received hourly, and included over 200 variables from each site with information on the local meteorological conditions, the surface fluxes, and the operational status of the systems. The GOES transmissions proved critical for identifying and diagnosing instrument problems, and, if necessary, dispatching a crew to the field.

The towers were designed to operate for long intervals without maintenance. The maximum interval between visits was dictated by the storage capacity of the memory cards used to store data. The raw turbulence data were archived at 4 Hz in summer, which allowed more than 6 weeks between visits, and 1 Hz in winter, which allowed more than 6 months between visits. The time between visits was also dictated by the likelihood of filter clogging, which was more common in summer due to forest fires.

We performed a sensitivity analysis to determine how the reduced sampling frequency in winter affected the calculated fluxes. Raw 4 Hz data collected in July 2004 at the 1964 site were resampled at lower frequencies, and the corresponding fluxes calculated using otherwise identical programs. The reduction in sampling frequency had a negligible effect on the calculated fluxes as indicated by the regression between 1 and 4 Hz flux (Table 3). The fluxes calculated at 1 Hz were on average 0.3% lower than those calculated at 4 Hz. The

Table 3 Effect of sampling frequency on calculated CO₂ exchange

Sampling frequency (Hz)	Slope	Intercept	r^2
4	1	0	1
2	1.0000	-0.0002	0.9991
1	1.0025	0.0077	0.9934
0.5	1.0088	0.0031	0.9386

Raw 4 Hz observations collected at the 1964 site in July 2004 were resampled at lower frequencies, and the resulting eddy covariance fluxes compared with the fluxes calculated with the original 4 Hz data.

lower winter sampling frequency reduced the number of samples from 7200 to 1800 per half hour, which increased the run-to-run variability as indicated by the r^2 values. The decrease in winter sampling frequency reduced the sample sizes but did not affect the response times of the instruments. The reduced sampling in winter therefore increased the run-to-run variability slightly, but did not cause a systematic bias in calculated flux.

Methods

Installation

We deployed eddy covariance towers at the 1850, 1930, 1964, 1981, and 1989 burns in July and August 2001, at the 1998 burn in June 2002, and at the 2003 burn in August 2003. Most of the equipment was assembled, sorted and packed into separate shipping cases at our home university and trucked to Manitoba. The equipment was then transported by helicopter into the five sites deployed in 2001 over the course of a day, working from a series of drop-off points along a gravel highway that paralleled the sites (Fig. 1). The installation of each site took 3–5 days, beginning with the power system and followed by the eddy covariance tower, instrument box, and cabling and grounding. The systems were then left to operate unattended, with scheduled or unscheduled visits every ~5 weeks in summer and ~3 months in winter.

Infrastructure

A typical site had four components (Fig. 2). (1) A scaffold tower that supported the solar panels (10 Siemens SR100 100-W panels, Siemens Solar Industries, Camarillo, CA, USA) and was typically ~50 m from the eddy covariance tower. The solar tower was constructed from steel scaffolding (Waco Industries or equivalent, Cleveland, OH, USA), and was tall enough to lift the bottom row of panels above the forest canopy. The scaffold stood on, and was guyed to, 4 in. diameter earth anchors augered 48 in. into mineral soil. The bottom row of panels was tilted to a 45° angle during the growing season and lowered into a vertical position during winter. (2) A polyethylene battery box (Hardigg Cases, South Deerfield, MA, USA) at the base of the solar scaffold that contained the main battery bank (16 Deka Gel 6-V, 180 A hr gel cell batteries wired to deliver 24 V, East Penn Manufacturing, Lynn Station, PA, USA), a charge controller (Trace Engineering C60, Arlington, WA, USA) and lightning protection (Polyphaser IS-24VDC-50A, Minden, NV, USA). (3) A 6–24 m fixed length or telescoping aluminum tower (Aluma Tower

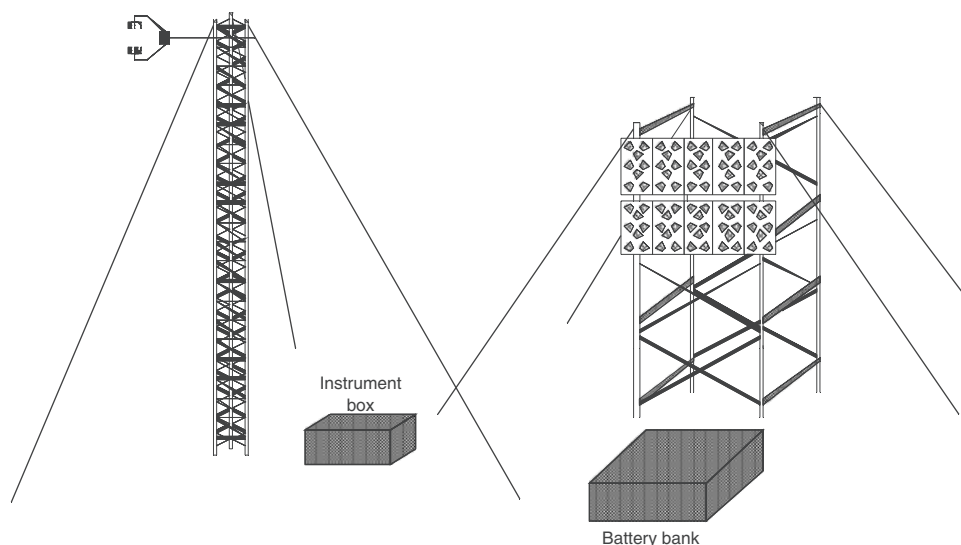


Fig. 2 A typical site showing the four main components. (1) A solar scaffold tower with 10 south-facing panels mounted vertically above the canopy. (2) A battery box containing 16 lead acid batteries at the base of the solar scaffold. (3) An eddy covariance tower that held the meteorological instruments ~ 4 m above the vegetation and that was located ~ 50 m from the solar scaffold. (4) An insulated instrument box at the base of the eddy covariance tower that contained the data logger, satellite radio, IRGA, and pump.

Company, Vero Beach, FL, USA or Heights Tower Systems, Pensacola, FL, USA) that supported the eddy covariance and meteorological instruments at ~ 4 m above the vegetation. (4) A polyethylene instrument box (Hardigg Cases) within 1–2 m of the base of the eddy covariance tower that contained the IRGA, pump, data logger, satellite radio, voltage regulator (ICT 2412-10A, Innovative Circuit Technology, Langley, BC, Canada), CO_2 calibration system, and lightning protection. The battery and instrument boxes were inset 15 cm or more into the soil to buffer their internal temperatures. The instrument boxes were insulated internally with 12.7 mm thick PVC and 12.7 mm thick polyethylene foam.

The 1850 and 2003 sites differed somewhat from the typical design. We used power at the 1850 site from a diesel generator that operated continuously at the nearby BOREAS Northern Study Area Old Black Spruce tower site (Table 2) to charge the battery bank with a charge controller, thus, eliminating the need for a scaffolding tower and solar panels. The 2003 site was installed after the study started, and budget limitations prevented us from equipping it for winter operation (the site had fewer batteries and the solar panels were mounted close to the ground).

Meteorological and eddy covariance flux measurements

The data acquisition and control system (CR5000, Campbell Scientific, Logan, UT, USA) was automated, allowing extended periods of unattended operation.

The raw data were archived on 1 Gb PCMCIA cards (1 Gb flashdisk, SanDisk, Sunnyvale, CA, USA). The data logger prepared two types of data files: (1) slow files with 30 min statistics and (2) fast files with raw 4 Hz data from a sonic and IRGA (1 Hz during the winter). The 30 min averages and covariances were stored on the PCMCIA cards and also transmitted via the GOES-West satellite every hour (SAT HDR GOES, Campbell Scientific). The final data sets are available from the authors (http://www.ess.uci.edu/~boreal_canada/index.html) and from the AmeriFlux Data Archive (<http://public.ornl.gov/ameriflux/data-access-select.shtml>). The raw data sets are available from the authors.

The turbulent fluxes of sensible heat, latent heat, CO_2 , and momentum were determined with the eddy covariance technique (Baldocchi *et al.*, 1988; Wofsy *et al.*, 1993). Wind and temperature were measured with a three-axis sonic anemometer (CSAT3, Campbell Scientific). The molar concentrations of CO_2 and H_2O at the tower top were measured with a closed-path IRGA (LI7000, LiCor). Air was drawn through two parallel 1 μm pore 47 mm diameter PTFE filters positioned near the sonic anemometer, down 4 mm inner diameter Teflon PFA tubing, and through a pleated stainless-steel filter (SS-4FW-2, Swagelok, Solon, OH, USA) by a brushless 12 V DC pump (N815, KNF Neuberger, Trenton, NJ, USA). The flow through the IRGA was measured with a mass flow meter (GFM17A-VADN2-A0A, Aalborg, Orangeburg, NY, USA). The IRGA reference cell was scrubbed of CO_2 and H_2O using a trap with

soda lime and $\text{Mg}(\text{ClO}_4)_2$. The IRGA was calibrated automatically for CO_2 once a week by sequentially sampling CO_2 and H_2O scrubbed air and CO_2 standard in air ($\pm 1\%$; Scott Marin, Riverside, CA, USA). The IRGA was calibrated manually for H_2O once every 3–6 months using a thermoelectrically driven condensing column (LI610, LiCor). The LI7000 molar concentrations on a dry air basis were recorded and corrected for calibration drift in subsequent processing.

The CO_2 fluxes were calculated as the 30 min covariance of the vertical wind velocity and the CO_2 mixing ratio after subtracting the 30 min mean. The time lag for the closed-path IRGA was determined by maximizing the correlation between the fluctuations in air temperature and CO_2 . The fluxes were rotated to the plane with no mean vertical wind (McMillen, 1988).

Observations of the physical environment were sampled at either 4 or 1 Hz. Precipitation was measured during above-freezing periods with a tipping bucket gauge (TE525WS, Texas Electronics, Dallas, TX, USA). Incoming and reflected photosynthetically active photon flux density (PPFD) was measured with silicon quantum sensors (LI190, LiCor). Net radiation was measured with a thermopile net radiometer ($Q^*7.1$, REBS, Seattle, WA, USA). Incoming and reflected solar radiation was measured with thermopile pyranometers (CM3, Kipp & Zonen, Delft, the Netherlands). Air temperature and relative humidity were measured with ventilated sensors (107, Campbell Scientific; HMP45C, Vaisala, Woburn, MA, USA; 077 radiation shield, MetOne, Grants Pass, OR, USA). Soil data were recorded every 2 h with a second data logger (CR-10X, Campbell Scientific). Soil temperatures in one or two profiles with eight depths from 1 to 100 cm beneath the soil surface were measured with thermistors (EC95H303W, Thermometrics, Edison, NJ, USA). Soil moisture at one to five locations from 2 to 70 cm beneath the soil surface was measured with horizontally positioned water content reflectometers (CS616, Campbell Scientific). Litter and moss moisture was measured using fuel moisture probes positioned in the litter and moss layers (CS505, Campbell Scientific).

Leaf area index (LAI)

The herbaceous, understory, and overstory LAIs at each site were determined in September 2004 by harvest or allometry using site-specific allometric equations and specific leaf areas (SLA). The herbaceous biomass in 30–40, 0.25 m² plots at 10 m intervals along 100 m transects radiating in the cardinal directions from the eddy covariance towers was clipped, returned to the lab, dried at 65 °C, and weighed. The herbaceous material was mostly leaves, and the SLAs from Bond-Lamberty

et al. (2002b) were used to calculate the herbaceous LAI at each site. The herbaceous LAI was partitioned into deciduous and evergreen leaves by sorting subsamples. The species composition and basal diameter of the understory shrubs or tree saplings in a series of 1 m² plots along the transects was measured with vernier calipers. Overstory tree diameters at breast height (DBH; 1.3 m) were measured in three or four 25–50 m² plots in the cardinal directions from the eddy covariance tower at each site with loggers tape (Original Loggers Tape, Spencer Products Co., Seattle, WA, USA). The understory and overstory foliage biomass and LAI of each species at each site was calculated with site-specific allometric equations from Bond-Lamberty *et al.* (2002a) and SLAs from Bond-Lamberty *et al.* (2002b).

Remote sensing

We used a time series of 16-day composite MODIS vegetation index images at 250 m resolution (MOD13Q1; Huete *et al.*, 2002) to determine whether our sites were representative of the region. We started with 200 km × 200 km images in Hierarchical Data Format (HDF) centered on the 1850 burn site, which we downloaded from the MODIS Validation Core Site website (<http://landval.gsfc.nasa.gov/coresite.php?SiteID=8>). We reprojected these images into the Universal Transverse Mercator (UTM) projection system using the HDF-EOS to GIS Format Conversion Tool (HEGTool, http://eosweb.larc.nasa.gov/PRODOCS/misr/tools/geotiff_tool.html), and imported the resulting HDF files into ENVI (The Environment for Visualizing Images; Research Systems Inc., Boulder, CO, USA). We then identified a series of regions of interest (ROI), which included 5 pixel × 5 pixel (1250 m × 1250 m) blocks around each tower, and also 27 larger areas of known age covering a total of 14 937 pixels with 81–2218 pixels each that we referred to as ‘survey sites’. The ages of the survey sites were determined from the Canadian Large Fire Database (http://cwfis.cfs.nrcan.gc.ca/en/historical/ha_lfdb_maps_e.php), using historic Thematic Mapper (TM) and Enhanced Thematic Mapper Plus (ETM+) images to delineate burn boundaries. We output the enhanced vegetation index (EVI) for the pixels in each ROI to an ASCII file, which we then imported into Matlab or Excel for analysis. EVI is considered less susceptible to biases associated with aerosols and soil reflectance than the more commonly used normalized difference vegetation index (NDVI; Huete *et al.*, 2002).

We also prepared a time series of midsummer (June–August) TM and ETM+ images for each year from 1984 to 2005 except 1988, which we used to test the space-for-time substitution. We acquired Landsat 5 TM

images for 1984–1996 from the BOREAS archive (http://www.eosdis.ornl.gov/BOREAS/boreas_home_page.html); Landsat 7 ETM+ images for 1999–2002 from the MODIS Validation Core Site website (<http://landval.gsfc.nasa.gov/coresite.php?SiteID=8>); and Landsat 5 TM images for 1997, 1998, and 2003–2005 from the US Geological Survey, Earth Resources Observation Science data archive (<http://eros.usgs.gov/>). We georeferenced each image in ENVI relative to a 1991 image that we took as our base. We output the at-sensor radiances for all bands for ROIs that included all tower sites, and imported the resulting ASCII files into Matlab. We cross-calibrated each image relative to the 1991 image using ~ 20 pseudoinvariant calibration targets, which included deep lakes that served as stable dark targets and rock outcrops and gravel pits that served as bright targets (Hall *et al.*, 1991). Finally, we calculated the time series of EVI (Huete *et al.*, 2002) for each ROI after converting radiance to surface reflectance taking the solar spectrum into account.

Results and discussion

Mesonet performance

The climate in central Manitoba is continental boreal, with extremely cold winters and mild to warm summers (Fig. 4a). The seasonal pattern of CO₂ exchange was closely related to air temperature, with photosynthesis and increased respiration from \sim May to \sim September, and very low rates of respiration from \sim November to \sim April (Fig. 3). The instrument boxes maintained internal temperatures of 10–20 °C throughout the winter despite the extreme cold (data not shown). The summer days were long and bright (Fig. 4b), providing ample sunlight to charge the batteries and allowing the equipment to run nearly continuously from March to October (Fig. 4c). In contrast, the winter days were short and dim, with insufficient light to maintain a safe charge on the batteries, which caused the systems to frequently switch the pumps and IRGAs off to conserve power (the other instruments continued to operate during most of these periods).

The six year-round sites were fully operational for $\sim 90\%$ of the growing season (Fig. 5a). Most of the missing CO₂ flux data in the growing season was caused by low battery charge or bad signals from the sonic anemometer. The six year-round sites were fully operational for $\sim 70\%$ of the dormant season, with most of the missing data caused by low battery charge (Fig. 5b). Additional noteworthy causes of missing data were a battery bank explosion that resulted from hydrogen accumulation, and ice plugs in the IRGA sample tubes that restricted flow. These problems, as well as

lost data caused by a loose wire, resulted from one-time events that were subsequently corrected and did not reappear. The continuity of summer data is typical for well-maintained eddy covariance sites (Falge *et al.*, 2001). The data were less continuous in the winter, with significant missing periods from November to January (Fig. 4c). The CO₂ exchange during the dormant period was uniformly low and consistent from day to day (Fig. 3). We feel the loss of data during some winter periods is a reasonable tradeoff given the cost and difficulty of installing the much larger battery banks that would have been needed for continuous winter operation.

Are the sites representative?

An eddy covariance tower integrates over a few hectares. Our mesonet of seven towers was an unusually dense deployment of eddy covariance instruments, but still sampled less than 0.01% of the approximately 250 000 ha shown in Fig. 1. Micrometeorologists have seldom directly addressed the question of whether their sites are representative (but see Hollinger & Richardson, 2005; Oren *et al.*, 2006), though it is important if observations are to be useful for regional and global problems. Remote sensing provides a valuable tool for assessing whether a site is representative (Roberts *et al.*, 2004). Micrometeorology provides rich data sets that document the exchanges of energy and mass by individual sites, but almost no information on how these individual sites compare with others that are not sampled. Remote sensing provides a powerful tool for comparing one site with another, but almost no direct information on the exchanges of energy and mass by the land surface.

The midsummer trend in EVI (Huete *et al.*, 2002) as a function of time since burn at the tower sites was generally similar to that observed at the broader collection of survey sites (Fig. 6a). The EVIs at the older sites (1850 and 1930), as well as the 2003 site in the years before burn, were ~ 0.3 . The EVIs immediately following burn dropped to 0.15, and then recovered rapidly over the next ~ 10 years to 0.4. The EVIs then increased more gradually to a maximum of 0.45 at the 1981 burn, before declining to 0.35–0.4 at the 1964 burn and ~ 0.3 at the older stands. The midsummer rates of CO₂ exchange measured by eddy covariance (Fig. 6b) paralleled the midsummer EVIs (Fig. 6a), underscoring the utility of EVI as a proxy for canopy gas exchange.

While the general trends were similar between the tower and survey sites, most of the individual tower sites deviated somewhat from the broader survey (Fig. 6a). The midsummer EVIs at the 1989, 1964, 1930, and 1850 sites were less than was observed for comparably aged stands in the broader survey. The

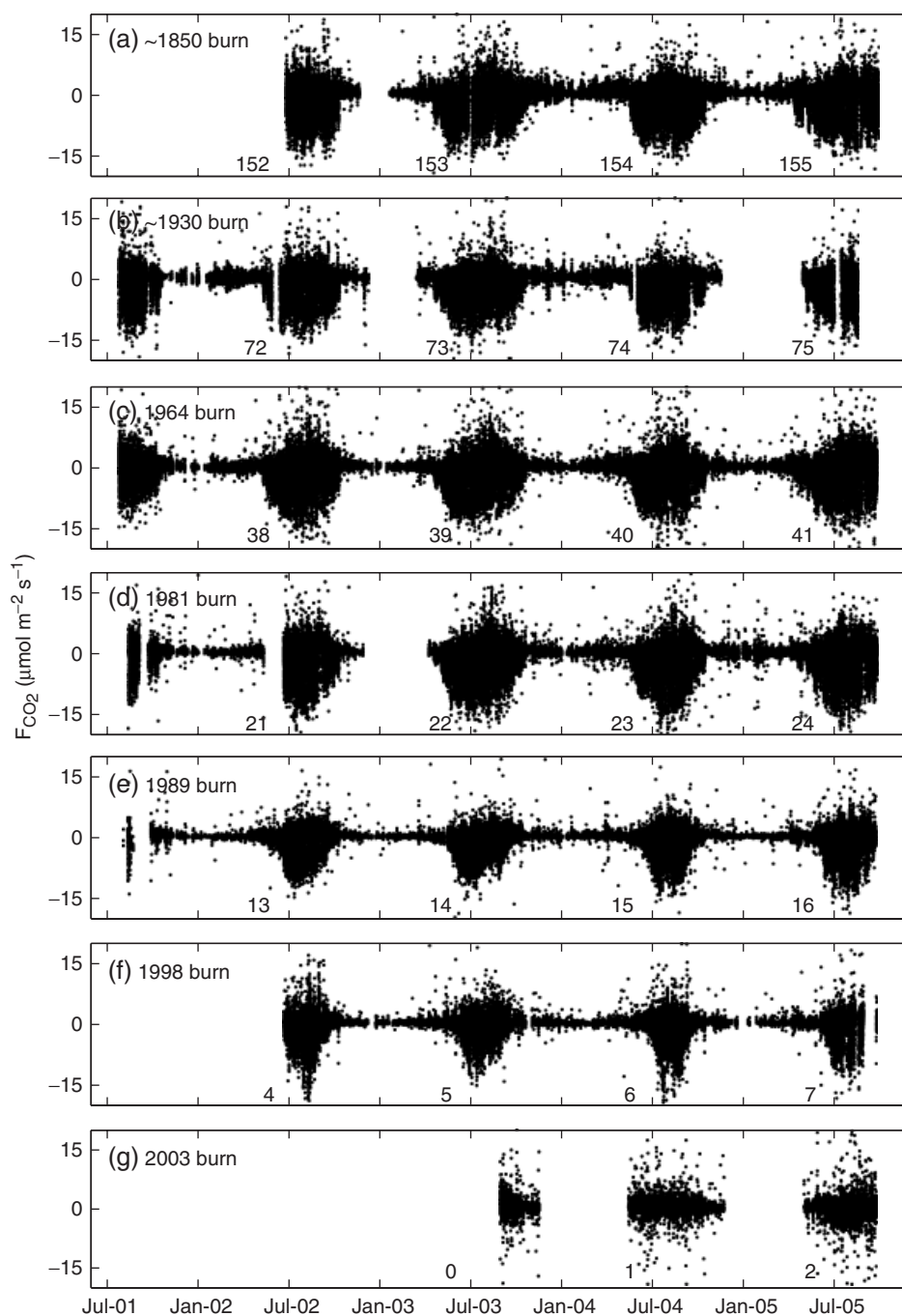


Fig. 3 Net CO_2 exchange determined by eddy covariance (F_{CO_2} ; $\mu\text{mol m}^{-2} \text{s}^{-1}$) from ~August 2001 to ~September 2005 at seven tower sites that last burned in (a) ~1850, (b) ~1930, (c) 1964, (d) 1981, (e) 1989, (f) 1998, (g) 2003. Individual points are half-hour covariances during both day and night with net negative fluxes indicating CO_2 uptake by the surface (photosynthesis) and positive fluxes indicating CO_2 loss (respiration). The upper envelope of points shows the seasonal pattern of nocturnal respiration; the lower envelope shows the seasonal pattern of net daytime CO_2 uptake; the difference between envelopes approximates the seasonal pattern of forest photosynthesis. Numbers indicate the age of each stand in each year.

midsummer EVI at the 1981 tower site was higher than was observed for comparably aged survey stands. The EVIs at the 1998 and 2003 tower sites were similar to those observed for comparably aged survey stands. We

conclude that our chronosequence provides a reasonable, though not perfect, representation of the broader patterns of fire recovery in the region. This comparison indicates that stand age is the main, but not sole, determinant of

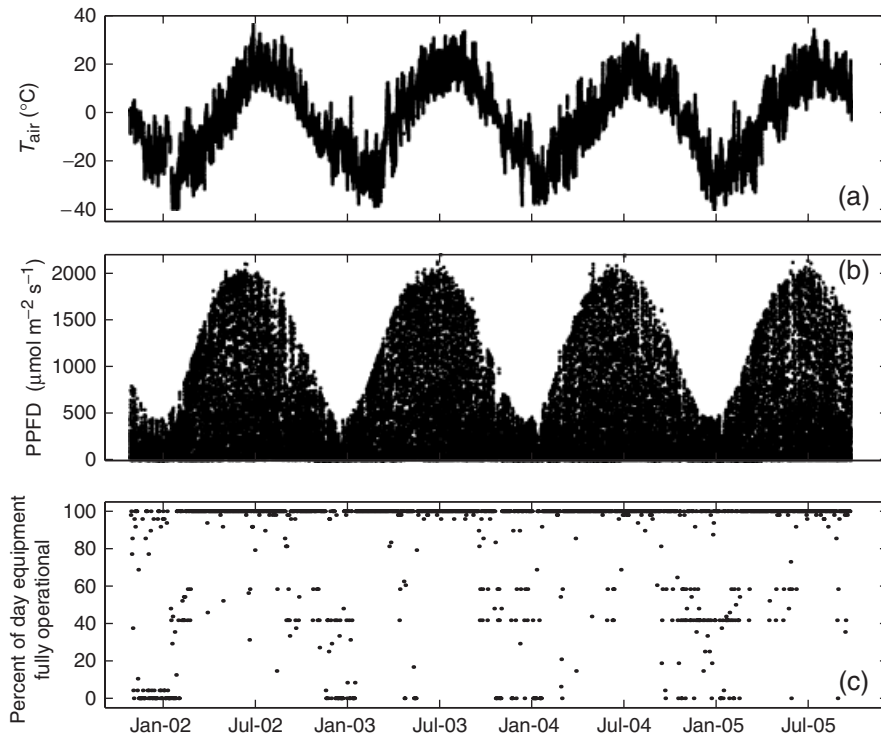


Fig. 4 Time series at the 1989 site of (a) air temperature (T_{air} ; °C), (b) incident photosynthetically active photon flux density (PPFD; $\mu\text{mol m}^{-2} \text{s}^{-1}$), and (c) the percent of time each day the equipment was fully operational.

EVI and canopy gas exchange among upland stands in the region, and that caution is needed when extrapolating observations from one boreal stand to another, even if the stands are nearby and of similar age (Table 2).

How quickly does midday peak gas exchange recover?

The midday rates of CO_2 exchange during the growing season recovered within 4 years of disturbance (Fig. 3). Peak midday CO_2 exchange at the 1998 burn was $10\text{--}15 \mu\text{mol m}^{-2} \text{s}^{-1}$ just 4 years after the fire. Similarly, the mean daytime CO_2 exchange during the growing season recovered to $\sim 6 \mu\text{mol m}^{-2} \text{s}^{-1}$ within 4 years of the fire, a rate that is only slightly less than that observed at most of the older stands (Fig. 6b). The rapid recovery was confirmed by the MODIS EVIs at both the tower and survey sites (Fig. 6a). The rapid reestablishment of productivity in boreal forest has been reported previously based on AVHRR (Amiro *et al.*, 2000; Hicke *et al.*, 2003) and Landsat (Epting & Verbyla, 2005) time series. Similarly, flux observations using aircraft and towers have confirmed that boreal forest resumes active CO_2 uptake within a few years of disturbance (Amiro *et al.*, 2003).

The fires killed nearly all of the trees and most of the shrubs and moss. The recovery of midday CO_2 uptake

was a result of the rapid reestablishment of leaf area by deciduous ruderals such as fireweed (Fig. 7, Table 1). The study sites differed in plant functional type (PFT), with the younger stands dominated by deciduous herbs and shrubs, and the older stands dominated by evergreen trees. The sites also contrasted in LAI, with an LAI of $2\text{--}3 \text{ m}^2 \text{ m}^{-2}$ in the younger stands (1989 and 1998) and an LAI of $5\text{--}7 \text{ m}^2 \text{ m}^{-2}$ in the older stands.

The patterns of PFT, LAI, gas exchange, and EVI raise several interesting issues. The convergence of CO_2 uptake among contrasting plant communities implies a tradeoff between leaf gas exchange and LAI, such that young, low LAI stands with rapidly photosynthesizing deciduous leaves achieve rates of canopy gas exchange that are comparable with those of old, high LAI stands with slowly photosynthesizing evergreen leaves. The consistency of gas exchange across sites suggests that an unidentified factor, such as average water availability, nitrogen mineralization, or light, colimits the ecosystem's photosynthetic capacity (Burke *et al.*, 1997; Hooper & Johnson, 1999). Assuming that this factor remains constant during succession, colimitation might account for the broadly constant rates of maximum and mean canopy photosynthesis that were independent of plant community composition. Finally, the correlation between EVI and canopy gas exchange over a wide

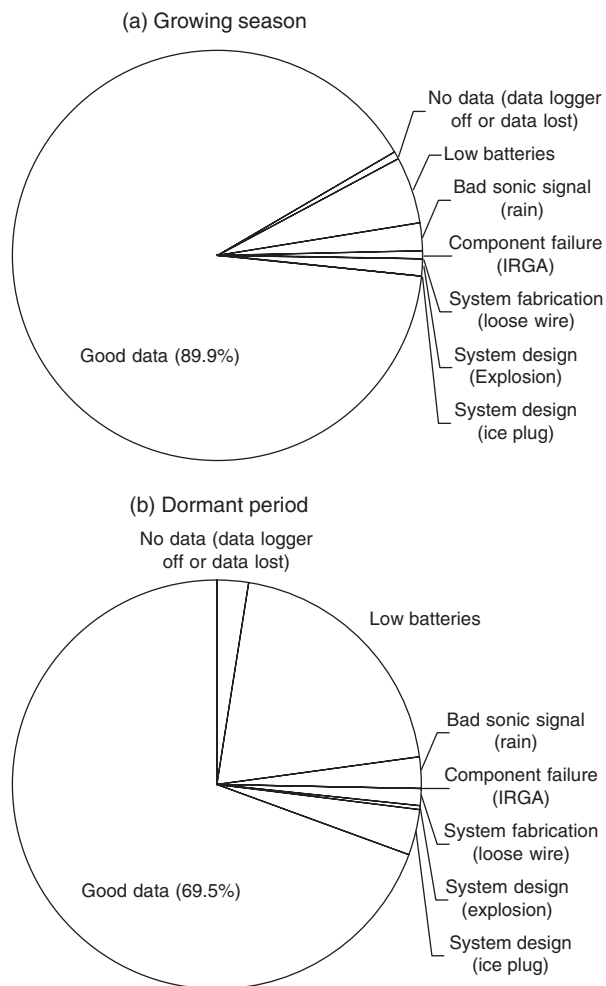


Fig. 5 Percent of time the CO₂ flux equipment at the 6-year-round sites (all sites except 2003 burn) was either fully operational ('Good data') or was missing as a result of several possible causes. The upper panel summarizes the data availability for the growing season [day of year (DOY) 140–271], and the lower summarizes the data availability for the dormant season (DOY 1–139 and 272–365), from September 2001 (the 1930, 1964, 1981, 1989 burn) or September 2002 (the 1850 and 1998 burns) until October 2004.

range of LAIs is consistent with past reports that EVI is more sensitive to deciduous leaves than evergreen ones (Chen *et al.*, 2005), and implies that the relationship between gas exchange and EVI (Fig. 6) is only partially related to LAI.

Is the space-for-time substitution valid?

Chronosequence studies assume the spatial patterns observed within a few years study are comparable with the patterns that would have been observed if a single site were observed continuously for a long period. We

tested the space-for-time substitution using a 22-year record of mid-growing season EVI for each site that we calculated from a collection of cross-calibrated Landsat TM and ETM+ images. The spatial patterns of mid-summer MODIS EVI (Fig. 6a) and eddy-covariance measured CO₂ flux (Figs 3 and 6b) implied that the trend in secondary succession by the tower sites can be divided into three phases: (1) a rapid recovery during the first few years following fire, (2) a gradual decrease from ~20 years after fire to ~75 years after fire, and (3) a constant EVI from approximately 75 years after fire to at least 150 years after fire. The initial EVI increase is almost certainly a result of the rapid proliferation of deciduous plants; the gradual decrease after ~20 years is likely a result of the increasing dominance of evergreen plants and the decline of deciduous leaf area (Chen *et al.*, 2005; Fig. 7). If the space-for-time substitution were valid, we would expect that individual stands have changed over the last 22 years in ways that match the spatially derived trends. For example, we would expect that the EVI at the 1989 burn increased markedly in the early 1990s, and the EVI at the 1964 burn decreased gradually from 1985 to 2005.

The TM and ETM+ time series (Fig. 8) confirmed that the study sites have changed over the last 22 years in ways that are consistent with the pattern inferred from the spatial observations (Fig. 6). The 1989, 1998, and 2003 sites all showed very rapid recovery during the first 2–3 years following fire, with increases of as much as 0.15 EVI units in a year. By contrast, the 1964 site showed a decline in EVI of 0.004 EVI units per year from 20 to 40 years after burn. Similarly, the 1930 site showed a decline in EVI of 0.003 EVI units per year from ~55 to ~75 years after burn. Finally, the ~1850 site had a generally consistent EVI from ~135 to ~155 years after burn. The 22-year time series at the individual sites yielded regressions that were broadly consistent with the other burns. For example, the time series at the 1930 burn was extrapolated back in time to estimate an EVI at age 40 that was broadly comparable with the EVI measured at the 1964 burn in 2004.

How does seasonality change during succession?

The seasonality of land-atmosphere exchange and growing-season length changed markedly with stand age (Fig. 3). The foliage in the younger stands (15 years and younger) was almost entirely deciduous (Fig. 7), which resulted in comparatively short peak growing seasons that lasted on average from day of year (DOY) ~175 (June 24) to DOY ~240 (August 28). In contrast, the older stands (22 years and older) were mostly evergreen, which resulted in comparatively long growing seasons that lasted from DOY ~140 (May 20)

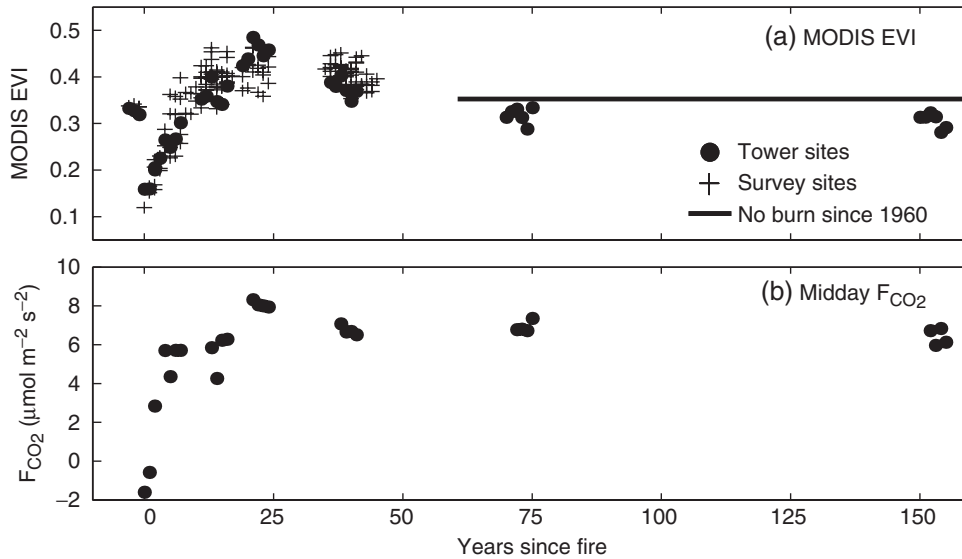


Fig. 6 (a) Midsummer [day of year (DOY) 177–256] MODIS enhanced vegetation index (EVI; unitless) as a function of years since most recent burn for the tower sites (\bullet) and for a separate survey of burns of known age ($+$). The horizontal solid line shows the mean EVI for survey stands with no reported burn since 1960. Symbols show the midsummer mean for each year at each tower or survey site. (b) Mean midday CO_2 uptake at each tower site averaged from 1500 Universal Time (UT) to 2000 UT for DOY 177–256 during periods with a friction velocity (u^*) greater than 0.2 m s^{-1} . A positive flux indicates increased CO_2 uptake by the vegetation, which is opposite the sign convention in Fig. 3.

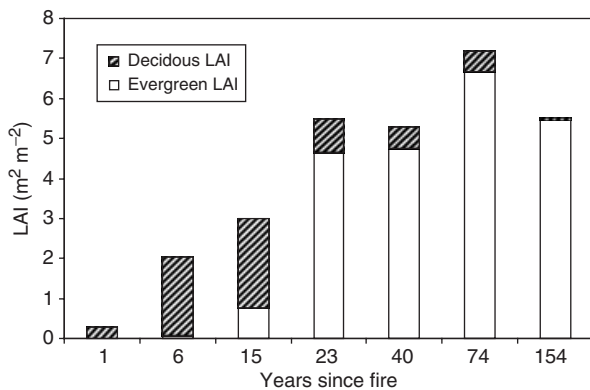


Fig. 7 Evergreen (open rectangle) and deciduous (cross hatched) Leaf Area Index (LAI; $\text{m}^2 \text{m}^{-2}$) at tower sites in September 2004.

to DOY ~ 270 (September 27). The marked shift in the seasonality of land–surface exchange during boreal succession has been reported previously (Roser *et al.*, 2002). Moreover, the trend from deciduous to evergreen foliage during secondary succession is well known (Van Cleve *et al.*, 1986), as is the relationship between phenology and the seasonal pattern of land–atmosphere exchange (Falge *et al.*, 2002).

A more detailed look at the temporal relationship between F_{CO_2} and air temperature underscores the

physiological basis of seasonality. Photosynthesis by evergreen stands began within a few days of the onset of above-freezing nocturnal conditions, and continued as long as daytime temperatures remained above freezing (Fig. 9a and b). Similar patterns were observed at all evergreen stands (Fig. 3), resulting in the nearly simultaneous onset and termination of gas exchange by stands that were 22 years old and older. The tight relationship between CO_2 exchange and air temperature (especially nocturnal temperature during spring and day temperature during fall) has been reported previously for NOBS (Goulden *et al.*, 1997) and European boreal forest (Tanja *et al.*, 2003). The springtime development of gas exchange by deciduous stands was delayed by the slow and gradual development of leaf area (Fig. 9c). The timing of the beginning and ending of the deciduous growing season was only weakly related to immediate weather thresholds. The deciduous growing season started in mid-June largely regardless of weather; the onset of deciduous senescence occurred in late August, coinciding with the arrival of colder weather (Figs 3 and 9).

The older stands had an average peak growing season that lasted ~ 130 days, which was twice as long as the younger stands' ~ 65 days growing season. The evergreen stands appear to exploit the maximum possible growing season given the constraint of below freezing temperature on photosynthesis (Figs 9a and b).

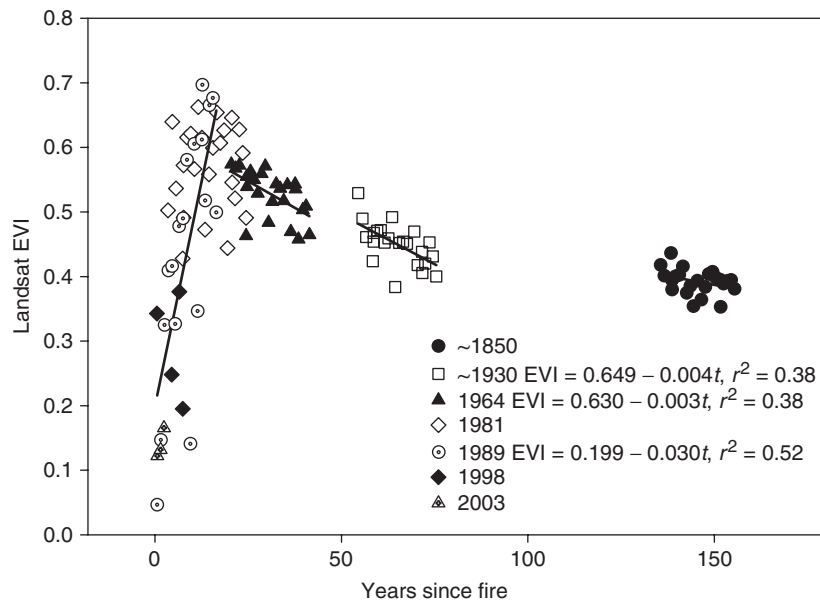


Fig. 8 Midsummer (June–August) enhanced vegetation index (EVI; unitless) as determined for each study site from Landsat Thematic Mapper (TM) and Enhanced Thematic Mapper Plus (ETM+) imagery. EVI is plotted as a function of time since burn, which was calculated by subtracting the year of last known burn from the image date. The first observation at the 1981, 1964, 1930, and 1850 sites was recorded in summer 1984. The last observation at each of the sites was recorded in summer 2005. Linear least squares regressions are shown for the 1930, 1964, and 1989 sites. The regressions at the other sites are not shown, either because there were few points (2003 and 1998 burn) or because EVI did not change systematically with time (1981 burn).

The difference in growing season length between deciduous plants and evergreen plants is likely a key controller of plant competition in boreal forests and a central driver of the changes in plant community composition during succession (e.g. Huston & Smith, 1987).

What other questions can an eddy covariance mesonet answer?

The first-year-round tower flux data sets were reported more than a decade ago from the Harvard Forest (Wofsy *et al.*, 1993), Walker Branch (Greco & Baldocchi, 1996), the BOREAS Southern Old Aspen site (Black *et al.*, 1996), and NOBS (Goulden *et al.*, 1997). These studies relied on a simple observational paradigm that we refer to as the single-year-round site experimental design. Year-round flux measurements at a single site were combined with *in situ* ecological measurements such as soil gas exchange; the eddy covariance fluxes were summed to calculate the annual carbon balance; the individual observations were interpreted from a plant ecophysiological perspective; the various types of data were combined to infer the controls on, and climatic sensitivity of, carbon, and energy exchange. The subsequent decade saw a proliferation of sites using the single-year-round site experimental design, along with the establishment of networks of individual sites such

as AmeriFlux, but only a limited focus on the development of more sophisticated experimental designs.

Long-term eddy covariance measurements made using the mesonet approach we describe should have good day-to-day, year-to-year, and site-to-site precision, even if the absolute accuracy of the half-hourly, and especially daily and annually integrated, flux is less certain (see also Goulden *et al.*, 1996, 2004; Morgenstern *et al.*, 2004). Ecologists have used a range of innovative experimental designs in the last century, such as controlled manipulations and gradient comparisons, that take advantage of a technique's site-to-site or temporal precision even when absolute accuracy is questionable. For example, controlled manipulations of the type used at Hubbard Brook (Bormann & Likens, 1979) are amenable to investigation with an eddy covariance mesonet. Alternatively, a mesonet of towers might be deployed along climatic (Jenny, 1941; Whittaker & Niering, 1975), vegetation, fertility (Pastor *et al.*, 1984), air pollution (Bytnerowicz & Fenn, 1996), urbanization, land use, or biological invasion (Vitousek *et al.*, 1987) gradients to better understand the controls on, and patterns of, land–atmosphere exchange. We encourage researchers to further explore clever and illuminating experimental designs that use eddy covariance's site-to-site and year-to-year precision to address pressing ecological, biogeochemical, hydrological, and meteorological issues.

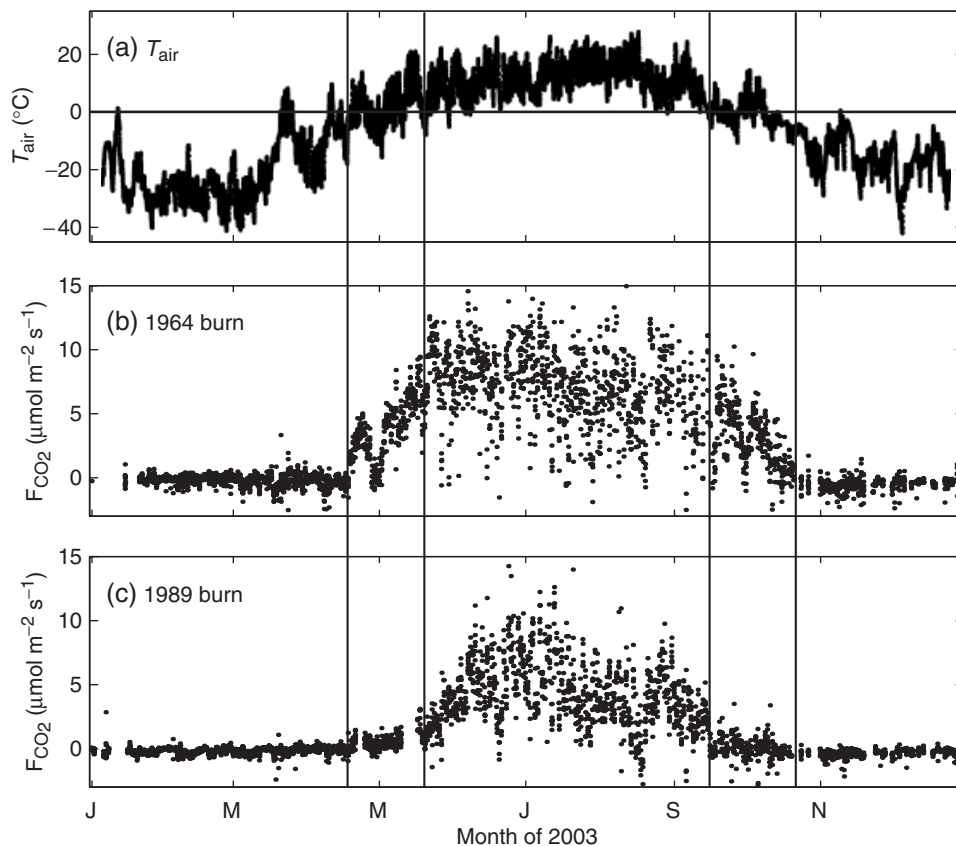


Fig. 9 (a) Air temperature at the 1964 burn site from January 1, 2003 to December 31, 2003. (b) Net CO_2 exchange (F_{CO_2} ; $\mu\text{mol m}^{-2} \text{s}^{-1}$) at the 1964 burn site from 1500 universal time (UT) to 2000 UT during periods with a friction velocity (u^*) greater than 0.2 m s^{-1} from January 1, 2003 to December 31, 2003. (c) Net CO_2 exchange at the 1989 burn site from 1500 to 2000 UT during periods with a u^* greater than 0.2 m s^{-1} from January 1, 2003 to December 31, 2003. A positive flux of CO_2 in (b) or (c) indicates greater land surface CO_2 uptake, which is opposite the sign convention in Fig. 3. Vertical lines show the beginning and end of active CO_2 uptake at the two sites.

Acknowledgements

We thank Scott Miller for help with data processing, and Steve Beaupre, Sami Rifai, Anders Holmberg, Aaron Fellows and Kelsey McDuffee for help in the field. We thank Steve Wofsy's lab at Harvard, Thompson Technologies, the NASA Terrestrial Ecology program, and the BOREAS science and support teams for setting up and operating NOBS. We thank Custom Storage, the Northern Lights Bed and Breakfast, the Churchill River Lodge, and Brad and Tara Ritchey for support, space, and friendship. We thank Tom Gower, Ben Bond-Lamberty, Sue Trumbore, Jennifer Harden, Steve Wofsy, Ali Dunn, and especially Hugo Veldhuis for sharing their understanding of the boreal forest. We thank The Nelson House First Nation Band and the Canadian Government for permission to work on their land. This work was supported by grants from the National Science Foundation, the Department of Energy, and the Comer Foundation.

References

- Amiro BD (2001) Paired-tower measurements of carbon and energy fluxes following disturbance in the boreal forest. *Global Change Biology*, **7**, 253–268.
- Amiro BD, Chen JM, Liu J (2000) Net primary productivity following forest fire for Canadian ecoregions. *Canadian Journal of Forest Research-Revue Canadienne De Recherche Forestiere*, **30**, 939–947.
- Amiro BD, MacPherson JI, Desjardins RL *et al.* (2003) Post-fire carbon dioxide fluxes in the western Canadian boreal forest: evidence from towers, aircraft and remote sensing. *Agricultural and Forest Meteorology*, **115**, 91–107.
- Baldocchi DD, Hicks BB, Meyers TP (1988) Measuring biosphere-atmosphere exchanges of biologically related gases with micrometeorological methods. *Ecology*, **69**, 1331–1340.
- Black TA, DenHartog G, Neumann HH *et al.* (1996) Annual cycles of water vapour and carbon dioxide fluxes in and above a boreal aspen forest. *Global Change Biology*, **2**, 219–229.
- Bonan GB, Shugart HH (1989) Environmental-factors and ecological processes in boreal forests. *Annual Review of Ecology and Systematics*, **20**, 1–28.
- Bond-Lamberty B, Wang C, Gower ST (2002a) Aboveground and belowground biomass and sapwood area allometric equations for six boreal tree species of northern Manitoba. *Canadian Journal of Forest Research-Revue Canadienne De Recherche Forestiere*, **32**, 1441–1450.

- Bond-Lamberty B, Wang C, Gower ST *et al.* (2002b) Leaf area dynamics of a boreal black spruce fire chronosequence. *Tree physiology*, **22**, 993–1001.
- Bond-Lamberty B, Wang CK, Gower ST (2004) Net primary production and net ecosystem production of a boreal black spruce wildfire chronosequence. *Global Change Biology*, **10**, 473–487.
- Bormann F, Likens GE (1979) *Pattern and Process in a Forested Ecosystem: Disturbance, Development, and The Steady State Based on The Hubbard Brook Ecosystem Study*. Springer-Verlag, New York.
- Brock FV, Crawford KC, Elliott RL *et al.* (1995) The Oklahoma mesonet – a technical overview. *Journal of Atmospheric and Oceanic Technology*, **12**, 5–19.
- Burba GG, Anderson DJ, Xu L *et al.* (2005) *Solving the off-season uptake problem: correcting fluxes measured with the LI-7500 for the effects of instrument surface heating progress*. Report of an ongoing study: Part I: Theory. Poster, AmeriFlux meeting, Boulder, CO.
- Burke IC, Lauenroth WK, Parton WJ (1997) Regional and temporal variation in net primary production and nitrogen mineralization in grasslands. *Ecology*, **78**, 1330–1340.
- Bytnerowicz A, Fenn ME (1996) Nitrogen deposition in California forests: a review. *Environmental Pollution*, **92**, 127–146.
- Chapin F, Matson PA, Mooney HA (2002) *Principles of Terrestrial Ecosystem Ecology*. Springer, New York.
- Chen X, Vierling L, Deering D *et al.* (2005) Monitoring boreal forest leaf area index across a Siberian burn chronosequence: a MODIS validation study. *International Journal of Remote Sensing*, **26**, 5433–5451.
- Clark KL, Gholz HL, Castro MS (2004) Carbon dynamics along a chronosequence of slash pine plantations in north Florida. *Ecological Applications*, **14**, 1154–1171.
- Cohen WB, Maersperger TK, Yang ZQ *et al.* (2003) Comparisons of land cover and LAI estimates derived from ETM plus and MODIS for four sites in North America: a quality assessment of 2000/2001 provisional MODIS products. *Remote Sensing of Environment*, **88**, 233–255.
- Dunn AL, Barford CC, Wofsy SC *et al.* (2006) A long-term record of carbon exchange in a boreal black spruce forest: means, responses to interannual variability, and long-term trends. *Global Change Biology*, doi: 10.1111/j.1365-2486.2006.01221.x
- Epting J, Verbyla D (2005) Landscape-level interactions of prefire vegetation, burn severity, and postfire vegetation over a 16-year period in interior Alaska. *Canadian Journal of Forest Research-Revue Canadienne De Recherche Forestiere*, **35**, 1367–1377.
- Falge E, Baldocchi D, Olson R *et al.* (2001) Gap filling strategies for defensible annual sums of net ecosystem exchange. *Agricultural and Forest Meteorology*, **107**, 43–69.
- Falge E, Baldocchi D, Tenhunen J *et al.* (2002) Seasonality of ecosystem respiration and gross primary production as derived from FLUXNET measurements. *Agricultural and Forest Meteorology*, **113**, 53–74.
- Gorham E, Vitousek PM, Reiners WA (1979) Regulation of chemical budgets over the course of terrestrial ecosystem succession. *Annual Review of Ecology and Systematics*, **10**, 53–84.
- Goulden ML, Daube BC, Fan SM *et al.* (1997) Physiological responses of a black spruce forest to weather. *Journal of Geophysical Research-Atmospheres*, **102**, 28987–28996.
- Goulden ML, Miller SD, da Rocha HR *et al.* (2004) Diel and seasonal patterns of tropical forest CO₂ exchange. *Ecological Applications*, **14**, S42–S54.
- Goulden ML, Munger JW, Fan SM *et al.* (1996) Measurements of carbon sequestration by long-term eddy covariance: methods and a critical evaluation of accuracy. *Global Change Biology*, **2**, 169–182.
- Goulden ML, Winston GC, McMillan AMS *et al.* Patterns of NPP, GPP, respiration and NEP during Boreal forest succession. In preparation.
- Gower ST, Vogel JG, Norman JM *et al.* (1997) Carbon distribution and aboveground net primary production in aspen, jack pine, and black spruce stands in Saskatchewan and Manitoba, Canada. *Journal of Geophysical Research-Atmospheres*, **102**, 29029–29041.
- Greco S, Baldocchi DD (1996) Seasonal variations of CO₂ and water vapour exchange rates over a temperate deciduous forest. *Global Change Biology*, **2**, 183–197.
- Hall FG, Strebel DE, Nickeson JE *et al.* (1991) Radiometric rectification – toward a common radiometric response among multirate, multisensor images. *Remote Sensing of Environment*, **35**, 11–27.
- Hicke JA, Asner GP, Kasischke ES *et al.* (2003) Postfire response of North American boreal forest net primary productivity analyzed with satellite observations. *Global Change Biology*, **9**, 1145–1157.
- Hollinger DY, Richardson AD (2005) Uncertainty in eddy covariance measurements and its application to physiological models. *Tree Physiology*, **25**, 873–885.
- Hooper DU, Johnson L (1999) Nitrogen limitation in dryland ecosystems: responses to geographical and temporal variation in precipitation. *Biogeochemistry*, **46**, 247–293.
- Huete A, Didan K, Miura T *et al.* (2002) Overview of the radiometric and biophysical performance of the MODIS vegetation indices. *Remote Sensing of Environment*, **83**, 195–213.
- Humphreys ER, Black TA, Morgenstern K *et al.* (2006) Carbon dioxide fluxes in three coastal Douglas-fir stands at different stages of development after harvesting. *Agricultural and Forest Meteorology*, in press.
- Huston M, Smith T (1987) Plant succession – life-history and competition. *American Naturalist*, **130**, 168–198.
- Jenny H (1941) *Factors of Soil Formation: A System of Quantitative Pedology*. McGraw-Hill, New York.
- Kasischke ES, Stocks BJ (2000) *Fire, Climate Change, and Carbon Cycling in the Boreal Forest*. Springer, New York.
- Kolari P, Pumpanen J, Rannik U *et al.* (2004) Carbon balance of different aged Scots pine forests in Southern Finland. *Global Change Biology*, **10**, 1106–1119.
- Law BE, Thornton PE, Irvine J *et al.* (2001) Carbon storage and fluxes in ponderosa pine forests at different developmental stages. *Global Change Biology*, **7**, 755–777.
- Litvak M, Miller S, Wofsy SC *et al.* (2003) Effect of stand age on whole ecosystem CO₂ exchange in the Canadian boreal forest. *Journal of Geophysical Research-Atmospheres*, **108**, 8225.

- McMillen RT (1988) An eddy-correlation technique with extended applicability to non-simple terrain. *Boundary-Layer Meteorology*, **43**, 231–245.
- Morgenstern K, Black TA, Humphreys ER *et al.* (2004) Sensitivity and uncertainty of the carbon balance of a pacific northwest Douglas-fir forest during an El Niño/La Niña cycle. *Agricultural Forestry Meteorology*, **123**, 201–219.
- Odum EP (1969) Strategy of ecosystem development. *Science*, **164**, 262.
- Oren R, Hsieh CI, Stoy P *et al.* (2006) Estimating the uncertainty in annual net ecosystem carbon exchange: spatial variation in turbulent fluxes and sampling errors in eddy-covariance measurements. *Global Change Biology*, **12**, 883–896.
- Pastor J, Aber JD, McLaugherty CA *et al.* (1984) Above-ground production and N and P cycling along a nitrogen mineralization gradient on Blackhawk Island, Wisconsin. *Ecology*, **65**, 256–268.
- Pregitzer KS, Euskirchen ES (2004) Carbon cycling and storage in world forests: biome patterns related to forest age. *Global Change Biology*, **10**, 2052–2077.
- Rapalee G, Trumbore SE, Davidson EA *et al.* (1998) Soil carbon stocks and their rates of accumulation and loss in a boreal forest landscape. *Global Biogeochemical Cycles*, **12**, 687–701.
- Roberts DA, Ustin SL, Ogunjemiyo S *et al.* (2004) Spectral and structural measures of northwest forest vegetation at leaf to landscape scales. *Ecosystems*, **7**, 545–562.
- Roser C, Montagnani L, Schulze ED *et al.* (2002) Net CO₂ exchange rates in three different successional stages of the “Dark Taiga” of central Siberia. *Tellus Series B – Chemical and Physical Meteorology*, **54**, 642–654.
- Schulze ED, Wirth C, Heimann M (2000) Climate change – managing forests after Kyoto. *Science*, **289**, 2058–2059.
- Sellers PJ, Hall FG, Kelly RD *et al.* (1997) BOREAS in 199: experiment overview, scientific results, and future directions. *Journal of Geophysical Research-Atmospheres*, **102**, 28731–28769.
- Sprugel DG (1985) Natural disturbance and ecosystem energetic. In: *The Ecology of Natural Disturbance and Patch Dynamics* (eds Pickett S, White P), pp. 335–352. Academic Press, New York.
- Tanja S, Berninger F, Vesala T *et al.* (2003) Air temperature triggers the recovery of evergreen boreal forest photosynthesis in spring. *Global Change Biology*, **9**, 1410–1426.
- Thornton PE, Law BE, Gholz HL *et al.* (2002) Modeling and measuring the effects of disturbance history and climate on carbon and water budgets in evergreen needleleaf forests. *Agricultural and Forest Meteorology*, **113**, 185–222.
- Van Cleve K, Chapin FS III, Flanagan PW *et al.* (1986) *Forest Ecosystems in the Alaskan Taiga: A Synthesis of Structure and Function*. Springer-Verlag, New York.
- Vitousek PM, Walker LR, Whiteaker LD *et al.* (1987) Biological Invasion by myrica-faya alters ecosystem development in Hawaii. *Science*, **238**, 802–804.
- Waring RH, Schlesinger WH (1985) *Forest Ecosystems: Concepts and Management*. Academic Press, Orlando.
- Webb EK, Pearman GI, Leuning R (1980) Correction of flux measurements for density effects due to heat and water-vapor transfer. *Quarterly Journal of the Royal Meteorological Society*, **106**, 85–100.
- Whittaker RH, Niering WA (1975) Vegetation of Santa Catalina Mountains, Arizona. 5. Biomass, production, and diversity along elevation gradient. *Ecology*, **56**, 771–790.
- Wofsy SC, Goulden ML, Munger JW *et al.* (1993) Net exchange of CO₂ in a midlatitude forest. *Science*, **260**, 1314–1317.